

Geometric Data Analysis based on Optimal Mass Transportation

Student

Simon Kai Hung Lam

Deerfield Academy
7 Boyden Ln
Deerfield MA 01342

Phone: (716) 398-2282

Email: slam19@deerfield.edu

Mentor

Xianfeng David Gu

Professor

Department of Computer Science
Department of Applied Mathematics
State University of New York at Stony Brook

Phone: (631) 632-1828

Email: gu@cs.stonybrook.edu

Geometric Data Analysis based on Optimal Mass Transportation

Simon Kai Hung Lam^a

^a*Deerfield Academy*

Abstract

3D shape classification plays a fundamental role in geometric big data analysis. This work proposes a novel method for shape classification based on optimal mass transportation theory. The Riemann surfaces are mapped onto canonical domains conformally based on uniformization theorem. The conformal factor function is treated as probability distribution on the canonical domain. For each pair of probability distributions, the optimal mass transportation map is computed by solving Monge-Amperé equation. The transportation cost is the Wasserstein distance between two distributions. By using this distance, geometric classification based on clustering can be performed. The method is applied to 3D human facial expression recognition, which demonstrates the efficiency and efficacy of the method.

Contributions

1. A novel geometric analysis method based on conformal mapping and optimal mass transportation theorem is proposed.
2. Efficient algorithms for discrete surface Yamabe flow and discrete optimal mass transportation map have been developed.
3. The method is verified by recognizing facial expressions using real 3D human facial surfaces.

5

Geometric Data Analysis based on Optimal Mass Transportation

Simon Kai Hung Lam^a

^a*Deerfield Academy*

Abstract

3D shape classification plays a fundamental role in geometric big data analysis. This work proposes a novel method for shape classification based on optimal mass transportation theory. The Riemann surfaces are mapped onto canonical domains conformally based on uniformization theorem. The conformal factor function is treated as probability distribution on the canonical domain. For each pair of probability distributions, the optimal mass transportation map is computed by solving Monge-Amperé equation. The transportation cost is the Wasserstein distance between two distributions. By using this distance, geometric classification based on clustering can be performed. The method is applied to 3D human facial expression recognition, which demonstrates the efficiency and efficacy of the method.

1. Introduction

1.1. Central Task

Recent years have witnessed the rapid development of 3D geometric acquisition technologies. Nowadays, the large scale geometric data sets are ubiquitous. Geometric data analysis plays an important role, which has great potentials to be applied in entertainment, security, finance, education, medicine and many fields in real life. In geometric analysis, geometric clustering is one of the most fundamental problems. In the current work, we propose an effective method for geometric clustering based on optimal mass transportation theory and apply it to human facial expression classification.

The 3D scanning system based on phase shifting structured light is capable of capturing dynamic facial surfaces with high speed and accuracy, which allows the system to capture 3D human facial expressions in real time. Fig. 1 shows one frame of the scanned human face viewed from three different angles. Fig. 2 illustrates the scanned facial surface with different expressions.

Problem 1.1 (Expression Classification). *How to find rigorous and efficient algorithms for classifying 3D human facial surface according to their expressions ?*



Figure 1: One 3D facial surface viewed from different angles.



Figure 2: The same facial surface with different expressions.

1.2. Conformal Mapping

A conformal mapping is an angle-preserving diffeomorphism, which maps a simply connected human facial surface onto the planar unit disk, such that the local shapes are well-preserved. Intuitively, in each neighborhood, the conformal map is a scaling transformation, but the scaling factor varies from point to point. As shown in Fig. 3, the conformal mapping maps infinitesimal circles to infinitesimal circles. The conformal mapping from the facial surface to the disk is not unique, as all conformal mappings differ by a Möbius transformation. By mapping the nose tip to the center, and the middle point of the inner eye corners to the imaginary axis, the mapping is unique. The area ratio between the infinitesimal disks is defined as the *conformal factor* function defined on the disk, the conformal factor can be treated as a probability measure. More

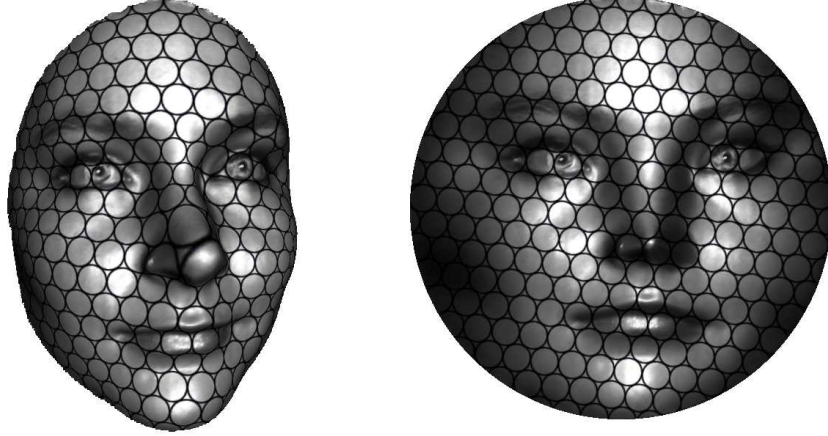


Figure 3: A conformal mapping from the 3D facial surface to the planar disk.

explicitly, suppose the human facial surface is denoted as (S, \mathbf{g}) where \mathbf{g} is the induced Euclidean metric, the conformal mapping is denoted as $\varphi : (S, \mathbf{g}) \rightarrow \mathbb{D}$, where \mathbb{D} is the unit planar disk $\mathbb{D} = \{|z| < 1 | z \in \mathbb{C}\}$. The mapping is conformal, then the metric has the representation

$$\mathbf{g}(z) = \lambda(z)dx \wedge dy = \lambda(z)\frac{i}{2}dz \wedge d\bar{z},$$

where $\lambda : \mathbb{D} \rightarrow \mathbb{R}$ is the conformal factor.

20 By this procedure, we can convert a 3D human facial surface (S, \mathbf{g}) to a probability measure $\lambda(z)\frac{i}{2}dz \wedge d\bar{z}$ defined on the planar unit disk.

1.3. Optimal Mass Transportation

The Optimal Mass Transportation theory offers a powerful tool to measure the distance between two probability measures. Suppose on a planar convex domain $\Omega \subset \mathbb{R}^2$, there are two probability measures μ and ν , with equal total mass $\mu(\Omega) = \nu(\Omega)$. A differential mapping $\varphi : \Omega \rightarrow \Omega$ is *measure-preserving*, if for any Borel set $B \subset \Omega$,

$$\int_{\varphi^{-1}(B)} d\mu = \int_B d\nu. \quad (1)$$

The measure-preserving condition is denoted as $\varphi_{\#}\mu = \nu$. The *transportation cost* for φ is defined as

$$\mathcal{C}(\varphi) := \int_{\Omega} c(p, \varphi(p))d\mu(p). \quad (2)$$

where $c(p, q)$ is the transportation cost for moving a point p to q . Among all the measure preserving mappings, the one that minimizes the transportation cost is called the *optimal mass transportation map*.

$$\varphi^* = \operatorname{argmin}_{\varphi_{\#}\mu = \nu} \mathcal{C}(\varphi). \quad (3)$$

The transportation cost of the optimal mass transportation map is called the *Wasserstein distance* between the two probability measures μ and ν

$$d_w(\mu, \nu) = \mathcal{C}(\varphi^*). \quad (4)$$

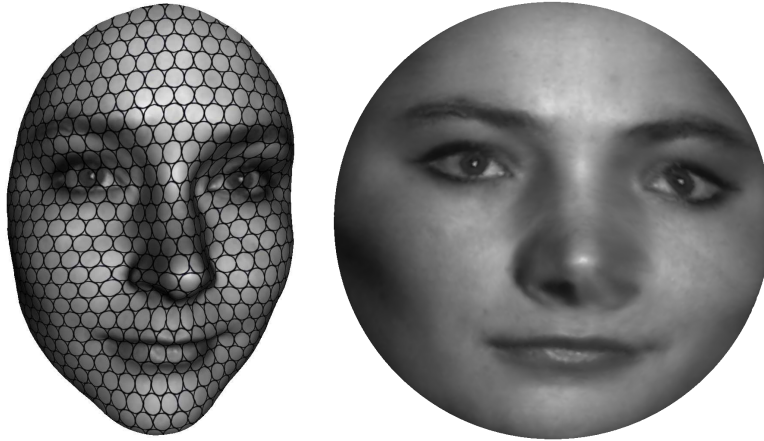


Figure 4: An area-preserving mapping from the facial surface onto the planar disk.

1.4. Proposed Method

In order to classify 3D human expression, we propose the following algorithmic pipeline:

1. The 3D human facial surfaces with different expressions are captured using 3D scanning system as described in [1]. Each facial surface is scaled to have the unit total area.
2. Each surface is conformally mapped onto the planar disk with the normalization condition. The conformal mapping induces conformal factor. Therefore, each facial surface with expression is converted to a probability measure.
3. For each pair of facial surfaces, compute the Wasserstein distance between the corresponding probability measures, which gives the shape distance between the facial surfaces.
4. Treat each facial surface as an abstract point and use shape distance for geometric clustering. Each cluster represents a expression.

2. Theoretic Background

In this section, we briefly introduce the theoretic foundation of our framework. We refer readers to [2] and [3] for detailed treatments.



Figure 5: 3D facial surfaces with different expressions captured using the 3D scanning system.



Figure 6: Same surfaces as in Fig.5, viewed from different angles.

40 *2.1. Conformal Mapping*

Suppose (S, \mathbf{g}) is a simply connected metric surface with a single boundary. Suppose a diffeomorphic map from the surface to a planar domain is $\varphi : S \rightarrow \mathbb{D}$, which parameterizes the surface. Assume the local parameters of \mathbb{D} is (u, v) , then the Riemannian metric has the form

$$\mathbf{g}(u, v) = e^{2\lambda(u, v)}(du^2 + dv^2),$$

where $\lambda : S \rightarrow \mathbb{R}$ is a smooth function, and φ is called a conformal mapping. A conformal mapping preserves angles and infinitesimal circles.

2.2. Surface Ricci Flow

Suppose (S, \mathbf{g}) is a closed surface with a Riemannian metric \mathbf{g} . Hamilton developed the surface Ricci flow, which deforms the Riemannian metric proportional to the Gaussian curvature, such that the curvature evolves according to diffusion-reaction equation, and eventually becomes constant everywhere. More explicitly, Hamilton's surface Ricci flow is defined as:

$$\frac{\partial g_{ij}(p, t)}{\partial t} = 2 \left(\frac{2\pi\chi(S)}{A(0)} - K(p, t) \right) g_{ij}(p, t),$$

where the metric tensor $\mathbf{g} = (g_{ij})$, K is the Gaussian curvature induced by the current
 45 metric, $\chi(S)$ is the Euler characteristic number of the surface, and $A(0)$ is the initial
 total area of the surface. Hamilton and Chow [4] proved that the surface Ricci flow
 converges to the constant curvature metric, the constant is $2\pi\chi(S)/A(0)$.

In our current work, we use the discrete surface Ricci flow. The existence of the
 solution to the flow and the uniqueness of the solution have been proved in [2].

50 2.3. Optimal Mass Transportation

In 18th century, Monge [5] raised the *optimal mass transportation problem*: how
 to find a measure preserving map that minimizes the transportation cost in Eqn. 2. In
 1940's, Kantorovich [6] introduced the relaxation of Monge's problem and solved it
 using linear programming. At the end of 1980's, Brenier [7] proved the following
 55 theorem.

Theorem 2.1 (Brenier). *Suppose the transportation cost is the quadratic Euclidean
 distance, $c(x, y) = |x - y|^2$. Given probabilities measures μ and ν on a convex domain
 $\Omega \subset \mathbb{R}^n$, then there is a unique optimal transportation map $T : (\Omega, \mu) \rightarrow (\Omega, \nu)$, fur-
 thermore there is a convex function $f : \Omega \rightarrow \mathbb{R}$, unique up to a constant, and the optimal
 60 mass transportation map is given by the gradient map $\phi : x \mapsto \nabla f(x)$.*

Assume the measures μ and ν are smooth, and f is with second order smoothness,
 $f \in C^2(\Omega, \mathbb{R})$. If f is measure-preserving, then it satisfies the Monge-Ampère equation.
 The two-dimensional Monge-Ampère equation is as follows:

$$\det \begin{pmatrix} \frac{\partial^2 f}{\partial x_1^2} & \frac{\partial^2 f}{\partial x_1 \partial x_2} \\ \frac{\partial^2 f}{\partial x_2 \partial x_1} & \frac{\partial^2 f}{\partial x_2^2} \end{pmatrix} = \frac{\mu(x_1, x_2)}{\nu \circ \nabla f(x_1, x_2)}. \quad (5)$$

In general, since Monge-Ampère equation is highly non-linear, conventional finite ele-
 ment method is incapable of solving this type of partial differential equation. Instead,
 [3] introduces a discrete method to solve it based on a convex optimization.

3. Computational Algorithms

65 In this section, we explain the computational algorithms in detail. There are two
 major algorithms: one computes the conformal mapping, while the other finds the
 optimal mass transportation map, and in turn, the Wasserstein distance.

3.1. Dynamic Discrete Surface Yamabe Flow

Suppose M is the input mesh with vertex, edge and face sets V, E, F respectively.
 70 We use v_i to represent a vertex, $[v_i, v_j]$ to represent the edge connecting v_i and v_j , and
 $[v_i, v_j, v_k]$ to represent the face consisting of the vertices v_i, v_j and v_k .

The *edge length* of $[v_i, v_j]$ is denoted as l_{ij} , the corner angle at v_i in triangle $[v_i, v_j, v_k]$
 is denoted as θ_i^{jk} . θ_i^{jk} can be obtained using cosine law:

$$\theta_i^{jk} = \cos^{-1} \frac{l_{ij}^2 + l_{ki}^2 - l_{jk}^2}{2l_{ij}l_{ki}} \quad (6)$$

The triangulation is *Delaunay*, if for each edge $[v_i, v_j]$ shared by two faces $[v_i, v_j, v_k]$ and $[v_j, v_i, v_l]$,

$$\theta_k^{ij} + \theta_l^{ji} \leq \pi.$$

The *discrete Gaussian curvature* at each vertex is defined as the angle deficit

$$K(v_i) = \begin{cases} 2\pi - \sum_{jk} \theta_i^{jk} & v_i \notin \partial M \\ \pi - \sum_{jk} \theta_i^{jk} & v_i \in \partial M \end{cases} \quad (7)$$

It can be easily shown that the discrete Gaussian curvature satisfies the discrete Gauss-Bonnet theorem:

$$\sum_{v_i \in V} K(v_i) = 2\pi\chi(M),$$

where $\chi(M) = |V| + |F| - |E|$ is the Euler characteristic number of the mesh. The *discrete conformal factor* is a function defined on the vertex set $u : V \rightarrow \mathbb{R}$. The edge length is given by

$$l_{ij} = e^{u_i} \beta_{ij} e^{u_j}, \quad (8)$$

where β_{ij} is the initial edge length. Given the target curvature $\bar{K} : V \rightarrow \mathbb{R}$ such that the target curvature satisfies the discrete Gauss-Bonnet theorem. The *discrete Yamabe flow* is defined as follows: for each vertex v_i ,

$$\frac{du_i}{dt} = \bar{K}(v_i) - K(v_i).$$

Initially, the conformal factor is set to be zero. The edge length induces the curvature K , and the flow deforms the conformal factor, changes the edge length, then the curvature in turn. It has been shown that the discrete yamabe flow is the gradient flow of the following Yamabe energy

$$E(\mathbf{u}) = \int^{\mathbf{u}} \sum_i (\bar{K}_i - K_i) du_i,$$

where \mathbf{u} is the vector representation of the conformal factors (u_1, u_2, \dots, u_n) . The gradient of the Yamabe energy is given by

$$\nabla E(\mathbf{u}) = (\bar{K}_1 - K_1, \bar{K}_2 - K_2, \dots, \bar{K}_n - K_n)^T. \quad (9)$$

It has been proven in [2] that the Yamabe energy is convex.

Given a triangulation of the vertices of the mesh M , we can construct its dual mesh \bar{M} as follows: for each face $f \in M$, its dual is a vertex $\bar{f} \in \bar{M}$ which is the circum-center of the face; for each edge $e \in M$ shared by two faces f_i and f_j , its dual is an edge $\bar{e} \in \bar{M}$ connecting circum-centers of f_i and f_j ; for each vertex $v \in M$, its dual is a face $\bar{v} \in \bar{M}$ consisting of the circum-centers of all the neighboring faces. We define the *edge weight* as follows: suppose the edge $[v_i, v_j]$ is shared by two faces $[v_i, v_j, v_k]$ and $[v_j, v_i, v_l]$, then

$$w_{ij} = \cot \theta_k^{ij} + \cot \theta_l^{ji}. \quad (10)$$

For Delaunay mesh, the edge weight is always non-negative. The Hessian matrix for the Yamabe energy can be formulated explicitly as

$$\frac{\partial^2 E(\mathbf{u})}{\partial u_i \partial u_j} = \begin{cases} -w_{ij} & v_i \sim v_j, i \neq j \\ 0 & v_i \not\sim v_j, i \neq j \\ \sum_k w_{ik} & i = j \end{cases} \quad (11)$$

From the Hessian formula, it is obvious that if the mesh is Delaunay, then on the hyperplane $\sum_i u_i = 0$, the Hessian matrix is positive definite, therefore the Yamabe energy is strictly convex. The solution is the unique global minimal point.

Given any target curvature \bar{K} satisfying the discrete Gauss-Bonnet theorem, one can use Yamabe flow to find the desired edge length. During the Yamabe flow, it may happen that some triangles are degenerated, therefore the flow has to terminate, and the solution cannot be obtained. In order to guarantee the existence of the solution we add one constraint to the flow: during the flow, the triangulation can be modified to be Delaunay all the time. At each time, the mesh is composed by gluing many Euclidean triangles. In generic cases, there is a unique Delaunay triangulation under this piecewise Euclidean metric, which can be obtained by simple edge swapping algorithm. Therefore, the dynamic Yamabe flow algorithm can be summarized in Alg. 1.

Algorithm 1: Dynamic Discrete Surface Yamabe Flow.

Input: The input mesh M and the target curvature \bar{K} , threshold ε
Output: The edge length which realizes the target curvature

- 1 Compute the initial edge lengths $\{\beta_{ij}\}$;
- 2 Initialize the conformal factor to be zeros;
- 3 **while true do**
- 4 Compute the edge lengths using Eqn.8;
- 5 Update the triangulation to be Delaunay by edge swapping;
- 6 Compute the corner angles using Eqn.6;
- 7 Compute the edge weights using Eqn.10;
- 8 Compute the vertex curvature using Eqn.7;
- 9 **if** $\forall |\bar{K}_i - K_i(\mathbf{h})| < \varepsilon$ **then**
- 10 | Break;
- 11 **end**
- 12 Compute the gradient of the Yamabe energy using Eqn.9;
- 13 Compute the Hessian of the Yamabe energy using Eqn.11;
- 14 Solve the linear system $Hess(\mathbf{u})\delta\mathbf{u} = \nabla E(\mathbf{u})$
- 15 $\mathbf{u} \leftarrow \mathbf{u} + \delta\mathbf{u}$;
- 16 **end**
- 17 **return** the edge length $\{l_{ij}\}$
- 18 ;

The dynamic Yamabe flow can handle meshes with low qualities. The existence of the solution has been proven in [2]. In our current work, we set the target curvature of the interior vertices to be zero everywhere, and the target curvatures of the boundary

vertices to be constant. After obtaining the target edge length, we can flatten the whole mesh face by face, such that the input simply connected mesh is mapped onto a planar convex domain.

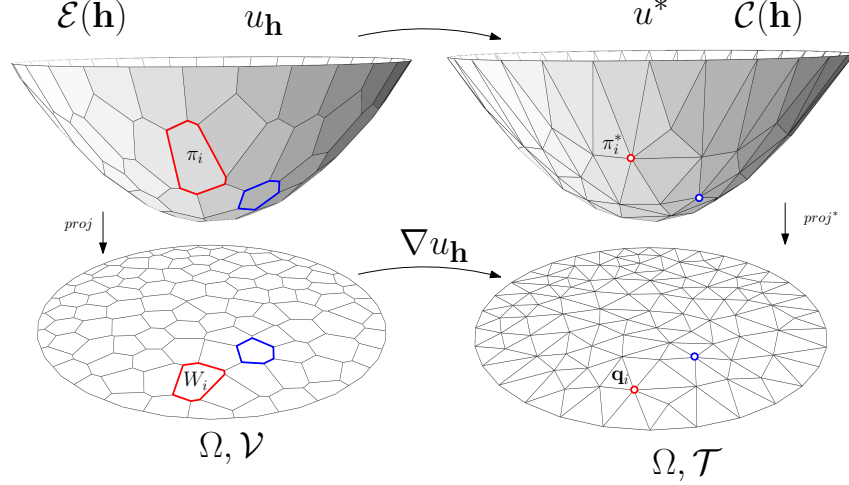


Figure 7: The upper envelope $\mathcal{E}(\mathbf{h})$ of $\{\pi_i(\mathbf{h})\}$ is the dual to the convex hull $\mathcal{C}(\mathbf{h})$ of $\{\pi_i^*(\mathbf{h})\}$. The projection of $\mathcal{E}(\mathbf{h})$ induces the power Voronoi cell decomposition $\mathcal{V}(\mathbf{h})$ of Ω . The projection of $\mathcal{C}(\mathbf{h})$ induces the power Delaunay triangulation $\mathcal{T}(\mathbf{h})$ of the discrete samples $\{\mathbf{q}_i\}$. The upper envelope $\mathcal{E}(\mathbf{h})$ is the graph of a piecewise linear convex function $u_{\mathbf{h}}$. The gradient map of the convex function $\nabla u_{\mathbf{h}}$ maps each power Voronoi cell $W_i(\mathbf{h})$ to a sample point \mathbf{q}_i .

90

3.2. Optimal Mass Transportation Map

In the current work, the source domain Ω is the canonical convex domain in \mathbb{R}^2 , the target is a set of discrete points $Y = \{\mathbf{q}_1, \mathbf{q}_2, \dots, \mathbf{q}_k\}$ which densely samples Ω . The source measure on Ω is represented by the conformal factor function μ . The target measure on Y is prescribed by the user, $\nu = \{v_1, v_2, \dots, v_k\}$, such that $\sum_{i=1}^k v_i$ is equal to the total area of Ω , $\int_{\Omega} d\mu$.

95

For each target point $\mathbf{q}_i \in Y$, we construct a plane in \mathbb{R}^3 , $\pi_i(\mathbf{h}, \mathbf{p}) := \langle \mathbf{q}_i, \mathbf{p} \rangle + h_i$, $i = 1, 2, \dots, k$. Then we compute the *upper envelope* of these planes.

3.2.1. Power Voronoi Diagram

For each plane $\pi_i(\mathbf{h})$, we construct a dual point $\pi_i^*(\mathbf{h}) \in \mathbb{R}^3$ as follows: assume the coordinates of $\mathbf{q}_i \in \mathbb{R}^2$ are (x_i, y_i) , then the dual point is $\pi_i^*(\mathbf{h}) = (x_i, y_i, -h_i)$, $i = 1, 2, \dots, k$. Then we compute the *convex hull* of $\{\pi_1^*(\mathbf{h}), \pi_2^*(\mathbf{h}), \dots, \pi_k^*(\mathbf{h})\}$ using incremental convex hull algorithm as described in [8], and denote the resulting convex hull as $\mathcal{C}(\mathbf{h})$. The boundary faces of $\mathcal{C}(\mathbf{h})$, whose normals are pointing downwards, form the lower part of the convex hull. We project the lower part of the convex hull $\mathcal{C}(\mathbf{h})$ to produce the *power Delaunay* triangulation of the point set Y , denoted as $\mathcal{T}(\mathbf{h})$.

105

The upper envelope of the planes $\{\pi_i(\mathbf{h})\}$ is denoted as $\mathcal{E}(\mathbf{h})$, which is the dual to the lower part of the convex hull $\mathcal{C}(\mathbf{h})$. We project the upper envelope onto the

(x, y)-plane to obtain the *power Voronoi diagram* of the plane. Each power Voronoi cell intersects Ω to obtain the *power Voronoi cell decomposition* of Ω , $\Omega = \cup W_i(\mathbf{h})$, denoted as $\mathcal{V}(\mathbf{h})$.

In fact, the upper envelope $\mathcal{E}(\mathbf{h})$ is exactly the graph of the convex function

$$G(\mathbf{h}, \mathbf{p}) = \max_{1 \leq i \leq k} \{\pi_i(\mathbf{h}, \mathbf{p})\}, \quad (12)$$

the power Voronoi diagram $\mathcal{V}(\mathbf{h})$ is the polyhedral partition of Ω by the gradient map of $G(\mathbf{h}, \mathbf{p})$, $\mathbf{p} \mapsto \nabla G(\mathbf{h})$.

3.2.2. Volume Energy

Let the area of each cell $W_i(\mathbf{h})$ in the power Voronoi cell decomposition $\mathcal{V}(\mathbf{h})$ be denoted as $w_i(\mathbf{h})$. We define the *admissible space* of the height vector as follows:

$$H := \left\{ \mathbf{h} \mid \sum_{i=1}^k h_i = 0, \forall 1 \leq i \leq k, w_i(\mathbf{h}) > 0 \right\}. \quad (13)$$

It can be proven that the admissible space is convex, as the details can be found in [3].

Furthermore, we define the *volume energy* on the admissible space as follows:

$$E(\mathbf{h}) = \int^{\mathbf{h}} \sum_{i=1}^k (v_i - w_i(\boldsymbol{\eta})) d\boldsymbol{\eta}_i. \quad (14)$$

The gradient of the energy is the difference between the target measure and the current cell area

$$\nabla E(\mathbf{h}) = (v_1 - w_1(\mathbf{h}), v_2 - w_2(\mathbf{h}), \dots, v_k - w_k(\mathbf{h}))^T. \quad (15)$$

We define the edge weight of the power Voronoi cell decomposition $\mathcal{V}(\mathbf{h})$ as follows: suppose $W_i(\mathbf{h})$ and $W_j(\mathbf{h})$ two adjacent cells, intersecting at the edge $e_{ij}(\mathbf{h})$

$$\lambda_{ij}(\mathbf{h}) = \frac{|e_{ij}(\mathbf{h})|_{\mu}}{|p_i - p_j|} \quad (16)$$

where

$$|e_{ij}(\mathbf{h})|_{\mu} = \int_{e_{ij}(\mathbf{h})} d\mu$$

The Hessian matrix of the volume energy is given by

$$\frac{\partial^2 E(\mathbf{h})}{\partial h_i \partial h_j} = \begin{cases} -\lambda_{ij}(\mathbf{h}) & W_i(\mathbf{h}) \sim W_j(\mathbf{h}), i \neq j \\ 0 & W_i(\mathbf{h}) \not\sim W_j(\mathbf{h}), i \neq j \\ \sum_k \lambda_{ik}(\mathbf{h}) & i = j \end{cases} \quad (17)$$

Because the edge weight is always positive, the volume energy is positive definite in the admissible space. The global maximizer of volume energy gives the power Voronoi cell decomposition $\mathcal{V}(\mathbf{h})$, in which the area of each cell $W_i(\mathbf{h})$ is equal to the desired measure v_i . Furthermore, the mapping $W_i(\mathbf{h}) \mapsto q_i$ is the gradient map of the convex function $G(\mathbf{h})$ and according to Brenier theorem, this mapping is the optimal mass transportation map.

3.3. Optimal Transportation Map Algorithm

In our current setting, the discrete point set Y is contained in the unit disk Ω . The initial height vector is set as follows: $h_i = \frac{1}{2}\langle \mathbf{q}_i, \mathbf{q}_i \rangle$, $i = 1, 2, \dots, k$. The initial power Delaunay triangulation $\mathcal{T}(\mathbf{h})$ is the traditional Delaunay triangulation, the power Voronoi cell decomposition of the unit disk is the traditional Voronoi cell decomposition.

At each step, we compute the power Delaunay triangulation $\mathcal{T}(\mathbf{h})$ and the power Voronoi cell decomposition $\mathcal{V}(\mathbf{h})$. The gradient of the volume energy in Eqn. 14 is given in Eqn. 15, and the Hessian of the volume energy is given by Eqn. 17. Then we solve the following linear equation

$$\nabla E(\mathbf{h}) = \left(\frac{\partial^2 E(\mathbf{h})}{\partial h_i \partial h_j} \right) \delta \mathbf{h} \quad (18)$$

with the linear constraint $\sum_{i=1}^k h_i = 0$, the solution exists and is unique. Then we can update the height vector by using Newton's method $\mathbf{h} \leftarrow \mathbf{h} + \lambda(\delta \mathbf{h})$, where λ is the step length parameter. In theory, the step length parameter should be chosen such that the height vector is kept inside the admissible space H (Eqn.13), namely, in the power Voronoi cell decomposition $\mathcal{V}(\mathbf{h})$ with each cell $W_i(\mathbf{h})$ being non-empty. In practice, in the middle of the optimization, we allow \mathbf{h} to exceed the admissible space H . The convexity of the volume energy automatically guides the height vector to return to the admissible space. The details of the algorithm can be found in Alg.2.

4. Experiment

We implemented proposed algorithms in Matlab. All the experiments are carried out on a Windows laptop with 2.3GHz dual core CPU and 8GB memory. We report our results in the following four subsections, which demonstrate that our algorithm allows users to classify 3D human facial expressions effectively.

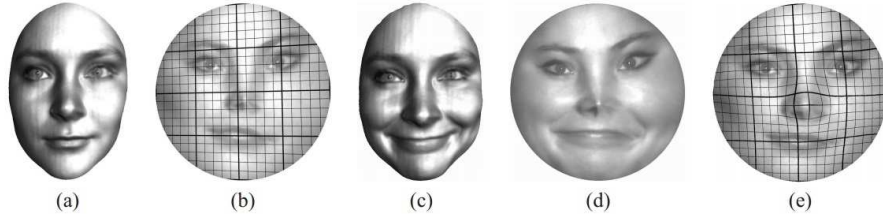


Figure 8: One 3D facial surface viewed from different angles.

The Wasserstein distance between two surfaces is a shape metric which can be used for quantifying shape differences. We use Alg.1 and Alg.2 to compute the Wasserstein distance. Fig. 8 shows the visualization results of Wasserstein distance. Figs. 8a and 8c are two face surfaces of different facial expressions. Figs. 8b and 8d are the conformal

Algorithm 2: Discrete Optimal Mass Transportation Map

Input: A convex domain $\Omega \subset \mathbb{R}^2$ and a set of discrete points $Y = \{\mathbf{q}_1, \dots, \mathbf{q}_n\}$,
discrete target measure $\mathbf{v} = \{v_1, \dots, v_n\}$, such that $\sum_i v_i = \text{Area}(\Omega)$

Output: A partition of Ω , $\Omega = \cup_i W_i$, such that $W_i \mapsto \mathbf{q}_i$ is the optimal mass
transportation map.

```
1 Translate and scale  $Y$ , such that  $Y \subset \Omega$ 
2 Initialize the height vector  $\mathbf{h}$ , such that  $h_i \leftarrow 1/2 \langle \mathbf{q}_i, \mathbf{q}_i \rangle$ 
3 while true do
4   for  $i \leftarrow 1$  to  $k$  do
5     Construct the plane  $\pi_i(\mathbf{h}) : \langle \mathbf{q}_i, \mathbf{p} \rangle + h_i$ 
6     Compute the dual point of the plane  $\pi_i^*(\mathbf{h})$ 
7   end
8   Construct the convex hull  $\mathcal{C}(\mathbf{h})$  of the dual points  $\{\pi_i^*(\mathbf{h})\}$ 
9   Compute the dual of the convex hull to obtain the upper envelope  $\mathcal{E}(\mathbf{h})$  of
   the planes  $\{\pi_i(\mathbf{h})\}$ 
10  Project  $\mathcal{C}(\mathbf{h})$  to obtain the power Delaunay triangulation  $\mathcal{T}(\mathbf{h})$  of  $Y$ 
11  Project  $\mathcal{E}(\mathbf{h})$  to obtain the power Voronoi cell decomposition  $\mathcal{V}(\mathbf{h})$  of  $\Omega$ 
12  for  $i \leftarrow 1$  to  $k$  do
13    Compute the area of  $W_i(\mathbf{h})$ , denoted as  $w_i(\mathbf{h})$ 
14  end
15  Construct the gradient Eqn. 15;
16  Construct the Hessian matrix Eqn. 17;
17  Solve the linear equation  $\text{Hess}(\mathbf{h})\delta\mathbf{h} = \nabla E(\mathbf{h})$ 
18   $\lambda \leftarrow 1$ 
19  Compute the power Voronoi diagram  $\mathcal{A}(\mathbf{h} + \lambda \delta\mathbf{h})$  of  $\Omega$ 
20  while  $\exists w_i(\mathbf{h} + \lambda(\delta\mathbf{h}))$  is empty do
21     $\lambda \leftarrow 1/2\lambda$ 
22    Compute the power Voronoi diagram  $\mathcal{A}(\mathbf{h} + \lambda \delta\mathbf{h})$  of  $\Omega$ 
23  end
24   $\mathbf{h} \leftarrow \mathbf{h} + \lambda \delta\mathbf{h}$ 
25  if  $\forall |w_i(\mathbf{h}) - v_i| < \varepsilon$  then
26    Break
27  end
28 end
29 return the mapping  $\{W_i(\mathbf{h}) \mapsto \mathbf{q}_i, i = 1, 2, \dots, k\}$ 
```

145 mapping results for Figs. 8a and 8c, respectively. Fig. 8e shows the optimal mapping from Figs. 8a to 8c, which induces Wasserstein distance. For better visualization of Fig. 8e, we put straight grids on Fig. 8c, and draw the deformed grids on Fig. 8e. From the grids deformation, we can clearly see how the surface around the mouth and nose deforms when the facial expression changes from calm to smile.



Figure 9: Expression classification by Wasserstein distance.

150 As noted earlier that Wasserstein distance can be used to quantify shape differences, we applied Wasserstein distance for facial expressions clustering. Our experimental dataset contains 10 people, each of which has three different facial expressions: “sad”, “happy” and “surprise” shown in Fig. 9 row 1, 2, 3, respectively. The 3D face surfaces are from Binghamton University 3D Facial Expression Database [9]. For each pair of surfaces in the dataset, we compute the Wasserstein distance.

155 Then we use classical multidimensional scaling (MDS) [10] to embed all 30 face surfaces in \mathbb{R}^2 based on the Wasserstein distance between each pair of faces. Fig. 10 illustrates the visualization results of the MDS embedding. For all the surfaces, we mark “sad” expressions as ‘+’ in blue color, and “happy” expressions as ‘x’ in red color, and “surprise” expressions as ‘o’ in green color. We can see that almost all faces with the same expressions are clustered together, and faces with different expressions are divided into different clusters. The facial expression clusters verify the idea that physical expressions of emotions can be systematically categorized and support the adoption to facial action coding system (FACS) [11] in computer vision and animation research. The experimental results also demonstrate the feasibility and potential of comparing and quantifying shape differences by conformal Wasserstein distance. More importantly, we anticipate that our approach may serve as novel shape distance for shape analysis.

5. Conclusions

170 This work proposes a method for geometric data analysis based on conformal mapping and optimal mass transportation theory and applies the method for 3D human

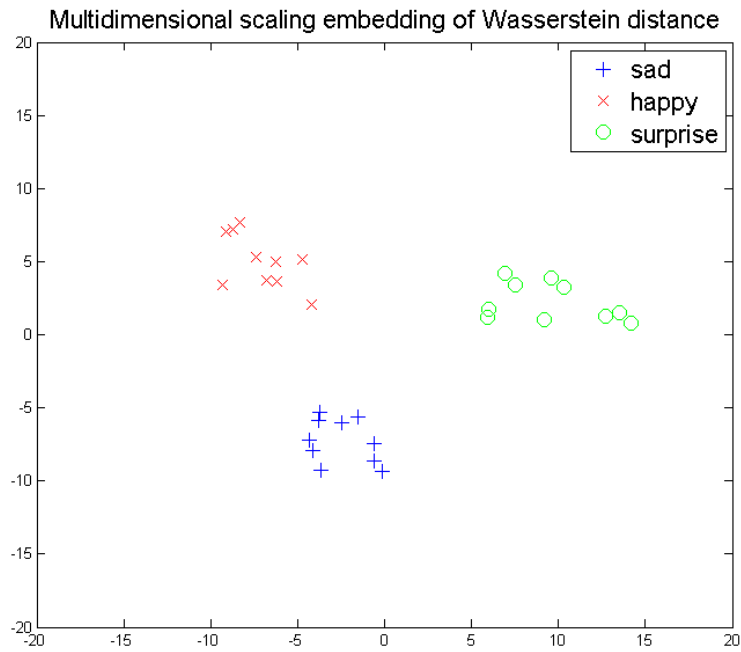


Figure 10: Multidimensional scaling embedding of the face surfaces using Wasserstein distance. .

facial expression classification. Our experimental results demonstrate the efficiency and efficacy of the proposed method.

175 The current method cannot handle surfaces with complicated topologies. In the future, we will generalize the proposed method for surfaces with more complicated topologies. Furthermore, we will apply this method to the recognition of subtle facial expressions.

References

- 180 [1] S. Zhang, S.-T. Yau, High-resolution, real-time 3d absolute coordinate measurement based on a phase-shifting method, *Optics Express* 14 (7).
- [2] X. Gu, F. Luo, J. Sun, T. Wu, A discrete uniformization theorem for polyhedral surfaces, arXiv:1309.4175.
- [3] X. Gu, F. Luo, J. Sun, S.-T. Yau, Variational principles for minkowski type problems, discrete optimal transport, and discrete monge-ampere equations, *Asian Journal of Mathematics(AJM)* 2 (20) (2016) 383–398.
- 185 [4] W. Zeng, X. D. Gu, *Ricci flow for shape analysis and surface registration: theories, algorithms and applications*, Springer Science & Business Media, 2013.
- [5] N. Bonnotte, From knothe’s rearrangement to brenier’s optimal transport map, *SIAM Journal on Mathematical Analysis* 45 (1) (2013) 64–87.
- 190 [6] L. Kantorovich, On a problem of monge, *Uspekhi Mat. Nauk.* 3 (1948) 225–226.
- [7] Y. Brenier, Polar factorization and monotone rearrangement of vector-valued functions, *Communications on Pure and Applied Mathematics* 44 (4) (1991) 375–417.
- [8] M. de Berge, O. Cheong, M. van Kreveld, M. Overmars, *Computational Geometry: Algorithm and Application*, 3rd Edition, Springer-Verlag, 2008.
- 195 [9] L. Yin, X. Chen, Y. Sun, T. Worm, M. Reale, A highresolution 3d dynamic facial expression database, *Int. Conf. Autom. Face and Gesture Recognit.* (2008) 17–19.
- [10] W. S. Torgerson, Multidimensional scaling: I. theory and method, *Psychometrika* 17 (1952) 401C419.
- 200 [11] P. Ekman, W. Friesen, Facial action coding system: A technique for the measurement of facial movement, *Consulting Psychologists*.